IEEE Access
Multidisciplinary : Rapid Review : Open Access Journal

Received November 17, 2016, accepted December 28, 2016, date of publication January 2, 2017, date of current version January 27, 2017.

Digital Object Identifier 10.1109/ACCESS.2016.2647226

Multi-Human Detection Algorithm Based on an Impulse Radio Ultra-Wideband Radar System

JEONG WOO CHOI, (Student Member, IEEE), SUNG SIK NAM, (Member, IEEE), AND SUNG HO CHO, (Member, IEEE)
Hanyang University, 04763 Seoul, South Korea

Corresponding author: S. H. Cho (dragon@hanyang.ac.kr)

S. S. Nam is a co-first author (email: ssnam@hanyang.ac.kr). This paper was presented at INTECH 2013, London, August 2013.
This work was supported by the ICT R&D program of MSIP/IITP [B0126-16-1018, The IoT Platform for Virtual Things, Distributed Autonomous Intelligence and Data Federation/Analysis].

ABSTRACT In this paper, we propose a multi-human detection algorithm based on impulse radio ultra-wideband radar system. With our proposed algorithm, the multi-human detection can be performed by repeatedly performing clustering and detecting processes. More specifically, the system detects an effective peak of the first single cluster which is composed of peaks adjacent to each other and then repeat this process until effective peaks of clusters caused by multiple people are successfully detected sequentially. As our performance metrics, we take into account the performance analysis in terms of the error probability based on the results of the statistical analysis. More specifically, we first cross-verify that the empirical result theoretically follows the Log-normal distribution by comparing the theoretical and empirical results obtained through laboratory experiments. Then, we statistically analyze the received signals under the Log-normal distribution assumption. After that, this statistical result is adopted to the performance analysis of the error probability in terms of the total error probability. Note that the performance of our proposed algorithm is affected by the threshold value. Based on it, the optimal threshold is analyzed and we provide the sample guidelines for optimally adjusting the threshold value under given various environment factors. Finally, some selected experimental results are presented to show the validity of our proposed algorithm by comparing the performance between the proposed algorithm and the conventional algorithm.

INDEX TERMS UWB, IR-UWB radar, multi-human detection, optimal threshold, CFAR, radar detection.

I. INTRODUCTION

Recently, the impulse radio ultra-wideband (IR-UWB) radar system has attracted significant attention in both scientific and commercial fields due to its remarkable advantages resulting from its extremely wide bandwidth such as good penetration, multipath immunity, and high-range resolution. In this regard, several research works based on IR-UWB system have been studied including indoor positioning, vital sign monitoring, people counting, and close range communications [1]–[8]. However, most studies related to human detection technologies are still limited to whether or not a target (a person or multiple people) is present or tracking the whereabouts of people, especially based on the given information about the number of people [9]–[16].

In general, the most well-known detection algorithm in radar systems including the IR-UWB radar is a constant false alarm rate (CFAR) algorithm [17], [18]. With the CFAR algorithm, a constant average false alarm rate can be maintained through an adaptive threshold control while maintaining an adequate target detection performance. However, it is difficult to directly apply a conventional CFAR algorithm to the real environment because the typical assumption of a homogeneous, Gaussian, and thermal noise-like background is routinely violated due to the spatial variation in clutter characteristics, and the effects of clutter edges which can leads performance degradation, etc.[1] Thus, modified CFAR algorithms have been proposed to effectively deal with the various types of backgrounds that are encountered (e.g., cell averaging CFAR (CA-CFAR) [17], order statistics CFAR (OS-CFAR) [18], greatest of CFAR, smallest of CFAR [20], [21], and selection and the estimation test [22]).

Although these algorithms can effectively deal with the various types of backgrounds, they are still inadequate for a multi-human detection scenario based on the IR-UWB radar system, especially, tracing each distance from multi-human, because these algorithms are valid in the variation detection

[1]The clutter is a term used for unwanted echoes mainly from non-human object, furniture, wall, and so on [19].

from the normal state to the active state of the signal (i.e., with these algorithms, it is available to detect only the presence or the absence of target regardless of the number of targets.). For multi-human detection case based on the IR-UWB radar system, many multipath signals caused by multi-human are appeared simultaneously and they are eventually combined into the form of multi-clusters with other clutter signals. As a result, with the conventional detection algorithm, the number of people can make it seem a lot more than it really is. Here, to detect multi-human correctly, actual main clusters caused by the actual people should be separated from received signals by neglecting other unwanted signals caused by the clutter and/or the multipath fading. However, unfortunately, with above mentioned algorithms, the system will detect all the multiple clusters and it eventually leads the difficulty of tracing each human.

Based on these motivations, we propose a new multi-human detection algorithm based on IR-UWB radar systems. With our proposed algorithm, the multi-human detection can be performed by detecting the effective peaks of multiple-clusters. More specifically, the system performs the detection process to find an effective peak of the first single cluster which is composed of peaks adjacent to each other and then repeat clustering and detecting processes until effective peaks of clusters caused by multiple people are successfully detected sequentially. As our performance metrics, we take into account the performance analysis in terms of the error probability according to both the threshold value and the signal level of the clutter based on the statistical analysis. Note that the performance of our proposed algorithm is affected by the threshold value. Based on it, the optimal threshold is analyzed and the sample guidelines for adjusting the threshold value at given various environment factors are provided. The main contributions of the paper are summarized as follows:

A. MAIN CONTRIBUTIONS

1. We propose a multi-human detection algorithm based on detecting an effective peak caused by actual people among clustered peaks adjacent to each other. In typical UWB channels, multipath components arrive at the receiver as the form of multi-clusters with other clutter signals [23]. With our proposed algorithm, the first step to detect the effective peaks is to find candidate peaks from signals in the form of multiple-clusters, and then by adopting the threshold crossing (TC) method [24], the system determines the effective peaks caused by actual people among them.
2. We cross-verify that the empirical result, which is measured in real environments, theoretically follows the Log-normal distribution by comparing the theoretical and empirical results in Fig. 1. [2] Then, we statistically analyze the received signals based on the IR-UWB radar system with our proposed algorithm under the Log-normal distribution assumption.

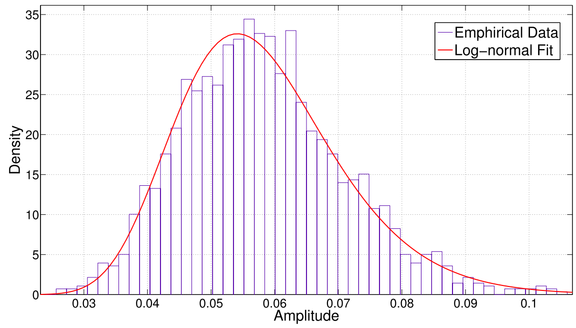

FIGURE 1. Comparison of the empirical amplitude statistic data with the theoretical fitting result.

3. As our performance metrics, we statistically analyze the error probability of our proposed multi-human detection algorithm in terms of the total error probability based on the results of the statistical analysis. More specifically, after dealing with two types of errors (i.e. false alarm and miss detection), we analyze the total error probability based on these two types of errors. Note that for the former case, a false alarm occurs if the system wrongly detects a target, while for the latter case, a miss detection occurs if no target is detected but the target(s) is(are) presented.
4. For practical consideration, the optimal threshold is analyzed and the sample guidelines about how to adjust the threshold value are presented for given various environment factors (e.g. path loss, shadowing, filter gain, and so on). Note that the performance of our proposed algorithm is affected by the threshold value due to the nature of the total error probability.[3] More specifically, to find only the effective peaks among several candidate peaks, the threshold needs to be increased to reject the effect of multipath and clutter signals. However, increasing the threshold level leads to increasing the probability of miss detection. Therefore, to adjust the threshold value optimally under given environments and to theoretically verify the performance optimization, we prove that there exists an optimal threshold which can minimize the error at given each environments and then we provide a sample guidelines about how to adjust the threshold value adequately under given environments.
5. Finally, some selected experiment results are provided to show the validity of our proposed algorithm by comparing the performance between the proposed algorithm and a conventional algorithm.

[2] Until now, various distributions, including the Rayleigh, Nakagami, Rice, Log-normal, and Gamma distributions, have been suggested for statistical analysis of the amplitude of the IR-UWB [23], [25]–[27].

[3] A false alarm occurs if the threshold is low enough to wrongly detects a target while a miss detection occurs if the threshold is high enough to miss the target when the target is presented.

II. SYSTEM AND CHANNEL MODEL

A received signal of the IR-UWB radar system can be represented as [28]

$$r_k(t) = \sum_{i=1}^{N_{\text{path}}} a_{ki} s\,(t - \tau_{ki}) + n(t), \tag{1}$$

where the subscript k means a slow time index representing the k-th received signal, and t means a fast time index representing the arrival time from the transmitting time. The subscript i indicates the i-th path from the transmitter to the receiver, $s(t)$ is the transmitted signal, and $n(t)$ represents the observation noise of the channel. a_{ki} and τ_i represent the scaling value and delay time of the k-th received signal through the i-th path, respectively. The received signal is composed of N_{path} scaled and delayed transmitted signals.

The received signal includes not only the desired signals reflected by the human, but also the unwanted signals reflected by the clutter. To remove these clutter signals, a background subtraction process need to be applied. The purpose of the background subtraction is to attenuate the clutter signals based on the degree of the signal's variation at each distance. If the variance of the signal is small, the probability that the signal is reflected by the clutter increases, and the signal is attenuated more than a signal that has large variance. There are several algorithms for the background subtraction, such as the algorithms using singular value decomposition (SVD), temporal median filter, and running average [29], [30]. Here, we apply the running average algorithm to evaluate the mean value as a clutter signal. This algorithm that subtracts the mean value as a clutter signal from an instantaneous received signal is frequently used because of the high performance and the relatively low computational complexity. The clutter-eliminated signal can be achieved by subtracting the clutter signal from the received signal as

$$\begin{aligned} c_k(t) &= \alpha c_{k-1}(t) + (1-\alpha) r_k(t), \\ y_k(t) &= r_k(t) - c_k(t), \end{aligned} \tag{2}$$

where $c_k(t)$ means the clutter signal, which can be estimated by applying the running average algorithm, $y_k(t)$ represents the background-subtracted signal, which mainly has the information for the samples with a large variance, and α is a parameter to adjust the application ratio of the received signal to the clutter signal.

If we set the value of α to be small, the clutter signal can be estimated quickly over a given new environment while the clutter signal is vulnerable to impulse noise because the instantaneous received signal has strong weight on estimating the clutter signal. However, for the larger value of α, a relatively longer time is needed to estimate the clutter signal but the clutter signal is subjected to relatively less impact on the impulse noise.

In (2), $y_k(t)$ includes clusters of multi-human. In the case of UWB, the channel measurements showed multipath arrivals in clusters rather than in a continuum, as is customary for narrowband channels [23]. This is caused by the fine resolution that UWB waveforms provide. Successive reflective paths can be individually resolved at the receiver, and that could result in a cluster of paths arriving at the receiver corresponding to reflections at a time, followed by a cluster of paths corresponding to other reflections. Even if there is a human, chest, head, and legs can make separate clusters.

III. MULTI-HUMAN DETECTION ALGORITHM

The main concerns of our proposed algorithm is how to separate the signal into multiple clusters, and how to find the effective peaks from the major clusters which are expected as being reflected by multi-human, not by the multipath or clutter from the background-subtracted signal which contains both multipath faded signals and clutter signals. In our proposed algorithm, candidate peaks are found from signals in the form of multiple-clusters, and then by adopting the threshold crossing (TC) method [24], the system determines the effective peaks which indicate the targets (i.e., human) among them. Here, the main (or important) issue in the multi-human detection algorithm is how to find these effective peaks while clustering the dense peaks in the form of sub-cluster. In our proposed algorithm, the received signal is divided into a number of coherent clusters in such a way that there is one representative local maximum peak in each coherent cluster. Here, this coherent cluster is determined by comparing each local peak with its adjacent local peaks in a recursive fashion. Then, this local maximum peak in each coherent cluster is considered as the candidate peak. Among these found candidate peaks, a number of peaks are determined as effective peaks of human using TC method. The detailed logic flow of our proposed new multi-human detection algorithm is summarized in Algorithm 1.

In Algorithm 1, t_{left} and t_{right} determine the spatial resolution of the clustering algorithm as the minimum distinguishable distance of two clusters. For small values of t_{left} and t_{right}, the signal is divided as more detail clusters, and we are able to distinguish two arbitrary human who are located more closely. However, it could raise the probability of finding much more number of effective peaks than the real number of people. As a result, it could make a confusion for the recognition of the number of target, and make it difficult to find distance traces of multi-human. In contrast, if we set the t_{left} and t_{right} as large values, multiple peaks within the parameters are regarded as being reflected by same body, and are clustered. Thus, only the maximum peak is considered as an effective peak. The clustering size is different from each cluster because of the condition of line 12 in Algorithm 1. The found peak between the descending or ascending peaks is not regarded as an effective peak based on the condition of line 12. The condition helps to keep the values of t_{left} and t_{right} small preventing the number of effective peaks from increasing meaninglessly. Instead of just finding the peak after the zero padding process, the condition of line 12 checks to see if the found peak is truly the local maximum in the initial ongoing signal, $d_0(t)$. To regard the found peak as

Algorithm 1 Multi-Human Detection Algorithm

procedure $(y(t))$
  $T \leftarrow$ threshold level
  $t_{left} \leftarrow$ left marginal time
  $t_{right} \leftarrow$ right marginal time
  $d_0(t) \leftarrow y(t)$ ▷ $d_0(t)$ is initial ongoing signal
  $A_{toa}(1:\text{end}) \leftarrow 0$ ▷ A_{toa} is ToA array
  $k \leftarrow 0$ ▷ k is peak counter
  $n \leftarrow 0$ ▷ n is iteration counter
  do
    $\hat{\tau}_n = \arg\max_t (d_n(t))$
    $\hat{a}_n = d_n(\hat{\tau}_n)$
    if $\hat{a}_n > \max\ y(\hat{\tau}_n - t_{left} : \hat{\tau}_n + t_{right})$ **then**
      $k = k + 1$
      $A_{toa}(k) = \hat{\tau}_n$
    end if
    $d_n(\hat{\tau}_n - t_{left} : \hat{\tau}_n + t_{right}) = 0$
    $d_{n+1}(t) = d_n(t)$
    $n = n + 1$
  while $\hat{a}_n > T$
  return $A_{toa}(1), A_{toa}(2), \ldots A_{toa}(k)$
end procedure

an effective peak, the found peak should meet the following two conditions as i) the amplitude must be greater than the threshold, T and ii) the peaks should be maximum value near the position of the peak in the initial ongoing signal, $d_0(t)$.

IV. STATISTICAL ANALYSIS

In this section, we statistically analyze the received signals which are measured in real environment that can be applied to the IR-UWB radar system with our proposed algorithm. While, in an IR-UWB radar system with wide bandwidth over 500MHz, it is well-known that the amplitude statistic of the received signal, a_{ki} in (1), follows the Rayleigh, Nakagami, Rice, log-normal, or Gamma distributions in literatures [23], [25]–[27], Fig. 1 shows that empirical result follows the log-normal distribution very well. Based on this observation, we cross-verify that the statistic of empirical results is theoretically equivalent to the log-normal distribution by comparing the theoretical and empirical results obtained through laboratory experiments. Note that in the following sections, we adopt the log-normal distribution for the performance analysis.

From the log-normal statistic of the amplitude data, we will drive other statistical parameters. $y_k(t)$ in (2), can be rearranged as

$$y_k(t) = \sum_{i=1}^{N_{\text{path}}} a'_{ki} s\left(t - \tau_{ki}\right) + n'(t), \tag{3}$$

where a'_{ki} and $n'(t)$ represent the modified amplitude of the k-th received signal through i-th path and the observation noise, respectively, after performing the background subtraction. The background-subtracted signal $y_k(t)$ is represented as a linear combination of successive received signals $r_k(t)$, $r_{k-1}(t)$, $r_{k-2}(t)$, ... and so on. Thus, the amplitude a'_{ki} is also a linear combination of $a_{ki}, a_{(k-1)i}, a_{(k-2)i}, \ldots$. Then, the statistic of a'_{ki} can be assumed as a log-normal random variable, because a_{ki} is the log-normal random variables, and the linear combination of log-normal random variables is assumed to be a log-normal random variable.

We regard the background subtraction as a kind of filter, and then we define the gain of the background subtraction filter as the ratio between the amplitudes of the received raw signal and the background subtracted signal. The filter gain G_{ki} can be written as

$$G_{ki} = a'_{ki}/a_{ki}, \tag{4}$$

where G_{ki} is a function of the parameter i, which means the i-th path of the received signal. This means that the gain G_{ki} is different from each path of the received signal. If the variance of the signal is large, the amplitude after the background subtraction also has large value because the background subtraction process passes a signal with large variance more intactly. Thus the filter gain G_{ki} has large value when a moving target, mainly human, exists. However, if there is little variation of the received signal, for the case in which only clutter exists, the filter gain G_{ki} has small value.

For the analytic convenience, we separate the signals in (1) and (3) into two parts as

$$\begin{aligned} r_k(t) &= \sum_{n=1}^{N_H} a_{kn} s\left(t - \tau_{kn}\right) + \sum_{m=1}^{N_C} a_{km} s\left(t - \tau_{kn}\right) + n(t), \\ y_k(t) &= \sum_{n=1}^{N_H} a'_{kn} s\left(t - \tau_{kn}\right) + \sum_{m=1}^{N_C} a'_{km} s\left(t - \tau_{kn}\right) + n'(t), \end{aligned} \tag{5}$$

where N_H and N_C represent the number of paths from the human and the clutter, respectively. The first and second parts of (5) represent the signal paths which are reflected by the human and clutter, respectively. If we define the filter gains for filtering the human signal and the clutter signal as G_H and G_C, respectively, then G_C and G_H can be written as

$$\begin{aligned} G_H &= a'_{kn}/a_{kn}, \\ G_C &= a'_{km}/a_{km}. \end{aligned} \tag{6}$$

We assume that G_C and G_H are stationary random variables over both time and path because these filter gains, G_C and G_H, are not functions of the time and the path (these values depends on the type of target for filtering). Here, based on the property of a log-normal random variable, G_C and G_H, which is represented as division with the two log-normal random variables, also have a log-normal characteristic. Therefore, the filter gains, G_C and G_H, follows a log-normal distribution.

V. PERFORMANCE ANALYSIS

In this section, as our performance metrics, we present performance analysis for our proposed multi-human detection algorithm. More specifically, the error probability is derived in terms of the total error probability based on the log-normal statistics. Here, the total error probability can be determined after dealing with both types of errors: a false alarm and miss detection. After dealing with two type of errors (false alarm and miss detection), we analyze the total error probability based on these two type of errors according to the amplitude of the clutter and the threshold value.

Before dealing with the error probability, for a tractable numerical analysis, we suggest one approximation. Although there could be several clutters in the signal of interest, analyzing the false alarm probability for the all of the clutters is inefficient. Most of the false alarm probability is determined by one major clutter, which has the largest amplitude, because we find multiple candidate peaks and determine which one is from human or clutter based on TC method. Then, there would be boundary between the peaks of the last human and the clutter. The clutter after the last human is a main concerns for analyzing the false alarm probability. Thus, analyzing the false alarm probability for the clutter that which has the largest amplitude is enough to consider the false alarm probability.

A. FALSE ALARM PROBABILITY

A false alarm occurs if the amplitude of the unwanted signal is greater than the threshold that is set for detecting a human when we use the proposed detection algorithm method. The unwanted signal is mainly constructed as a summation of the clutter and multipath signals of a human. Generally, if there is nothing except a non-moving clutter, the signal is very static, and the G_C has a very small value. However, if there is a human in the environment, many multipath signals are superpositioned with the clutter signals at the back side of a human, and that causes the filter gain of the clutter, G_C, to increase, because the multipath signal makes variations. Thus, to analyze the false alarm probability, we need to analyze the amplitude and filter gain of the clutter behind the human.

For convenience, we use the normalized amplitude of the clutter signal with the amplitude of the human instead of using the amplitude of the clutter and the human signal separately. The normalized amplitude of the human signal always equals 1, because the amplitude is normalized by itself. The normalized amplitude of the clutter signal can be written as

$$A = \frac{A_C}{A_H}, \tag{7}$$

where A_C and A_H are the amplitudes of the clutter and human, respectively. With this normalized parameter, the false alarm probability can be written as

$$P_F(T) = P\left(AG_C > T\right), \tag{8}$$

where AG_C means the background subtracted amplitude of the clutter and the false alarm occurs when AG_C is greater than the threshold T. Here, G_C follows a log-normal distribution where the mean and variance of the filter gain G_C are defined as m_{G_C} and v_{G_C}, respectively, and AG_C also follows a log-normal distribution where the mean and variance of AG_C are Am_{G_C} and $A^2 v_{G_C}$, respectively. Then, the false alarm probability can be evaluated as

$$\begin{aligned} P_F(T) &= \int_T^{\infty} \frac{1}{x\sigma_{G_C}\sqrt{2\pi}} e^{-\frac{\left(\ln x - u_{G_C} - \ln A\right)^2}{2{\sigma_{G_C}}^2}} dx, \\ &= 1 - \int_0^{T} \frac{1}{x\sigma_{G_C}\sqrt{2\pi}} e^{-\frac{\left(\ln x - u_{G_C} - \ln A\right)^2}{2{\sigma_{G_C}}^2}} dx, \\ &= \frac{1}{2} - \frac{1}{2}\mathrm{erf}\left(\frac{\ln T - u_{G_C} - \ln A}{\sqrt{2{\sigma_{G_C}}^2}}\right), \end{aligned} \tag{9}$$

where

$$u_{G_C} = \ln\left(\frac{(Am_{G_C})^2}{\sqrt{A^2 v_{G_C} + (Am_{G_C})^2}}\right),\ \sigma_{G_C} = \sqrt{\ln\left(1 + \frac{v_{G_C}}{{m_{G_C}}^2}\right)}.$$

If the threshold T increases, the value of (9) decreases due to the nature of the error function which is a monotonically increasing function. Increasing the threshold T means that it is more difficult for the filtered clutter signal to exceed the threshold. Thus, the false alarm probability should decrease. The false alarm probability has a negative correlation with the threshold T.

B. MISS DETECTION PROBABILITY

A miss detection occurs when the amplitude of the human signal is smaller than the threshold T. Thus, the miss detection probability P_M can be written as

$$P_M(T) = P\left(1 \times G_H < T\right), \tag{10}$$

where $1 \times G_H$ represents the filtered amplitude of the human signal, because the amplitude of the human is normalized by itself as 1. Here, G_H follows a log-normal distribution where the mean and variance are defined as m_{G_H} and v_{G_H}, respectively. Similar to (9), the miss detection probability can be solved as

$$\begin{aligned} P_M(T) &= \int_0^{T} \frac{1}{x\sigma_{G_H}\sqrt{2\pi}} e^{-\frac{\left(\ln x - u_{G_H}\right)^2}{2{\sigma_{G_H}}^2}} dx \\ &= \frac{1}{2} + \frac{1}{2}\mathrm{erf}\left(\frac{\ln T - u_{G_H}}{\sqrt{2{\sigma_{G_H}}^2}}\right), \end{aligned} \tag{11}$$

where $u_{G_H} = \ln\left(\frac{{m_{G_H}}^2}{\sqrt{v_{G_C} + {m_{G_C}}^2}}\right)$, $\sigma_{G_H} = \sqrt{\ln\left(1 + \frac{v_{G_H}}{{m_{G_H}}^2}\right)}$. Note that increasing the threshold T makes it difficult for the filtered human signal to exceed the threshold.

C. TOTAL ERROR PROBABILITY

The total error probability can be obtained based on the derived results of the two error cases: false alarm and miss detection. The two error cases can be assumed to be independent events, because a false alarm is related to the amplitude of the clutter signal, and the miss detection is related to the amplitude of the human signal. Here, the total error probability considers three cases: when one, a false alarm occurs, when a miss detection occurs, or when the two errors occur simultaneously. As results, the total error probability can be formulated as

$$P_E(T) = 1 - (1 - P_F(T))\,(1 - P_M(T))\,, \tag{12}$$

where $(1 - P_F(T))$ and $(1 - P_M(T))$ represent the probability of the complementary events of the false alarm and the miss detection, respectively. Then, the total error probability can be obtained based on the log-normal distribution as

$$P_E(T) = 1 - \left(\frac{1}{2} + \frac{1}{2}\mathrm{erf}\left(\frac{\ln T - u_{G_C} - \ln A}{\sqrt{2\sigma_{G_C}{}^2}}\right)\right) \times \left(\frac{1}{2} - \frac{1}{2}\mathrm{erf}\left(\frac{\ln T - u_{G_H}}{\sqrt{2\sigma_{G_H}{}^2}}\right)\right). \tag{13}$$

VI. PROOF OF OPTIMALITY

The total error probability curve in (13) always has an optimal value for a specific threshold value, T_{Opimal}, regardless of the parameters m_{G_C}, v_{G_C}, m_{G_H}, v_{G_H} and A. Especially, (13) has the shape of a quasiconvex function as shown in Fig. 2. To prove the quasiconvexity, we simplify (13), and we prove that the simplified equation satisfies the quasiconvexity. Then, we extend this result to prove the quasiconvexity of (13).

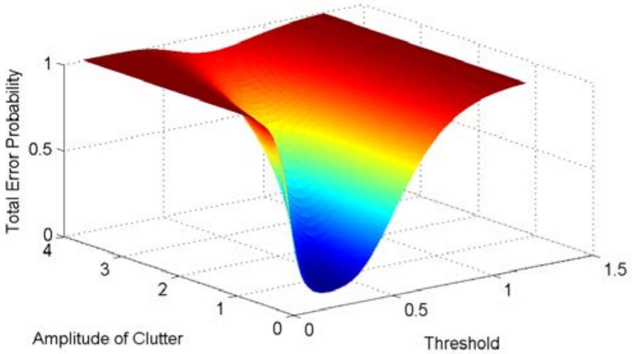

FIGURE 2. 3D plot of total error probability, $P_E(T)$ ($u_{G_H} = -0.3656$, $u_{G_C} = -1.4311$, $\sigma_{G_H} = 0.2779$, $\sigma_{G_C} = 0.3682$).

In (13), if we let $a = \frac{1}{\sqrt{2\sigma_{G_H}{}^2}}$, $b = \frac{u_{G_H}}{\sqrt{2\sigma_{G_H}{}^2}}$, $c = \frac{1}{\sqrt{2\sigma_{G_C}{}^2}}$, $d = \frac{u_{G_C} + \ln(A)}{\sqrt{2\sigma_{G_C}{}^2}}$, $f_{a,b}(x) = (-1 + \mathrm{erf}(a \ln x) - b)$, and $g_{c,d}(x) = (1 + \mathrm{erf}(c \ln x - d))$, then (13) can be simplified as

$$f_{a,b}(x) g_{c,d}(x) = (-1 + \mathrm{erf}(a \ln x - b)) \times (1 + \mathrm{erf}(c \ln x - d)) \text{ for } (a, c > 0), \tag{14}$$

where $x > 0$. (14) is a simply scaled and translated function of (13).

Here, without loss of generality, proving the quasiconvexity of (14) has the same meaning of proving the quasiconvexity of (13). In (13), these horizontal scaling multipliers (a and b) affect the domain but leave the range unchanged. More specifically, for $a \geq 1$ or $b \leq 1$, this horizontal scaling leads to a horizontal shrinking based on the value of a or b. Otherwise, a horizontal stretching occurs. Similarly, for c and d, c and d produce a horizontal scaling. As a result, these values change the shape/size (stretching and shrinking) of the graph of the function, but the overall trend of the graph is left unchanged. Therefore, in this sections, we consider the proof of the quasiconvexity of the simplified formula in (13), instead of the original formula in (14). More specifically, for analytical convenience, we prove the quasiconvexity of (13) with the specific case (e.g. $a = c = 1$ and $b = d = 0$) as

$$\begin{aligned} E(x) &= f_{1,0}(x) g_{1,0}(x), \\ &= (1 - \mathrm{erf}(\ln x)) \times (1 + \mathrm{erf}(\ln x)). \end{aligned} \tag{15}$$

To prove the quasiconvexity of (15), we apply the basic necessary and sufficient condition which a quasiconvex function has [31]. Consider any $p, q \in \mathbb{R}$ and any $\lambda \in (0, 1)$. Assume, without loss of generality, that $p > q$. Then we need to prove that $E(\lambda p + (1 - \lambda) q) \leq \max\{E(p), E(q)\}$ for quasiconvexity. Suppose that $E(p) \geq E(q)$, which means that $(\mathrm{erf}(\ln p))^2 \geq (\mathrm{erf}(\ln q))^2$, so that, given that the error function is a monotonically increasing function, it is obvious that $(\mathrm{erf}(\ln p))^2 \geq (\mathrm{erf}(\ln(\lambda p + (1 - \lambda) q)))^2$. Similarly, if we suppose that $E(q) \geq E(p)$, then $(\mathrm{erf}(\ln q))^2 \geq (\mathrm{erf}(\ln p))^2$, proving that $(\mathrm{erf}(\ln q))^2 \geq (\mathrm{erf}(\ln(\lambda p + (1 - \lambda) q)))^2$. As results, both inequalities show that (15) is a quasiconvex function, which directly means that the total error probability is a quasiconvex function based on the properties of the parameters a, b, c, and d.

VII. OPTIMAL THRESHOLD

In this section, the optimal threshold is evaluated by applying the bisection method [32] numerically for given environment factors. The optimization problem is equivalent with the following problem:

$$\begin{aligned} &\text{minimize } P_E(T), \\ &\text{subject to } T > 0. \end{aligned}$$

In Table I, the optimal threshold values based on the typical indoor channel conditions are given as a sample example where the parameter A means the amplitude of the most critical clutter normalized by the amplitude of a human in the signal of interest. This sample example in Table I shows the sample guidelines for the optimal threshold value for detecting multi-human with our proposed algorithm based on given environmental factors if the normalized amplitude A of the clutter is given. [4] The statistical parameters m_{G_H}, v_{G_H}, m_{G_C} and v_{G_C} are calculated based on our laboratory experiments (we obtain experimental data based on the IR-UWB radar system with our proposed algorithm implemented using an NVA-R661 evaluation board.).

The statistical parameters, such as σ_{G_H}, u_{G_H}, σ_{G_C}, and u_{G_C} in (9) and (11), vary with the channel conditions. σ_{G_H} and σ_{G_C} are relevant to the shadowing effect of the channel [33]. If the

[4]The normalized amplitude of the clutter can be estimated or measured empirically in the environment.

TABLE 1. The optimal threshold and related error probability for given environment factors.

The optimal threshold and related error probability for given environment factors with $m_{G_H} = 0.8004$, $v_{G_H} = 0.0783$, $m_{G_C} = 0.1641$, and $v_{G_C} = 0.0026$.													
A	0.15	0.2	0.25	0.3	0.35	0.4	0.45	0.5	0.55	0.6	0.65	0.7	0.75
T_{Optimal}	0.1205	0.1404	0.1581	0.1742	0.1891	0.2030	0.2161	0.2286	0.2405	0.2519	0.2629	0.2735	0.2837
P_E	6.13e-08	6.83e-07	3.88e-06	1.47e-05	4.26e-05	0.0001	0.0002	0.0004	0.0007	0.0011	0.0018	0.0026	0.0037
A	0.8	0.85	0.9	0.95	1	1.05	1.1	1.15	1.2	1.25	1.3	1.35	1.4
T_{Optimal}	0.2937	0.3034	0.3128	0.3219	0.3309	0.3396	0.3482	0.3566	0.3648	0.3729	0.3808	0.3886	0.3962
P_E	0.0051	0.0068	0.0088	0.0112	0.0141	0.0173	0.0210	0.0252	0.0298	0.0173	0.0404	0.0465	0.0529
A	1.45	1.5	1.55	1.6	1.65	1.7	1.75	1.8	1.85	1.9	1.95	2	2.05
T_{Optimal}	0.4038	0.4112	0.4185	0.4257	0.4328	0.4398	0.4467	0.4535	0.4603	0.4670	0.4735	0.4801	0.4865
P_E	0.0599	0.0673	0.0751	0.0834	0.0921	0.1011	0.1105	0.1203	0.1304	0.1408	0.1516	0.1625	0.1737
A	2.1	2.15	2.2	2.25	2.3	2.35	2.4	2.45	2.5	2.55	2.6	2.65	2.7
T_{Optimal}	0.4929	0.4992	0.5054	0.5116	0.5177	0.5237	0.5297	0.5357	0.5416	0.5474	0.5532	0.5589	0.5646
P_E	0.1852	0.1968	0.2086	0.2206	0.2327	0.2449	0.2572	0.2696	0.2820	0.2945	0.3070	0.3196	0.3321

shadowing effect is severe due to the many reflection paths, the parameter values σ_{G_H} and σ_{G_C} increase. The increase in σ_{G_H} causes the parameter values a and b to decrease, and it eventually leads the performance degradation. This means that if the shadowing effect on the human's signal is more severe, the signal of the human is more scattered and the detection probability decreases which leads the performance degradation.

Moreover, u_{G_H} and u_{G_C} are relevant to the degree of path loss of the channel [33]. The severe path loss effect causes these parameters to increase. An increase in u_{G_H} lowers the error probability and an increase in u_{G_C} makes the error probability increase.

In addition to the effect of the channel conditions, the optimal threshold is also affected by the filter gains, G_H and G_C, respectively. These filter gains could vary with the degree of movement of the target, although the target has the same radar cross-section (RCS). If a human is moving with a large motion, the filter gain can be slightly increased, because the filter attenuates only the static signal, and then, an increase of the filter gain of the human improves the performance.

Note that the above insight of properties of the optimal threshold with the different channel conditions can provide the guidelines or potential solutions about how to set the optimal threshold to achieve the desired error probability at a given environment.

VIII. EXPERIMENT RESULTS

To show the validity of our proposed algorithm, we conducted experiments using the IR-UWB radar system made by NOVELDA in Norway. The name of the board is NVA-R661. Center frequency and -10dB bandwidth are 6.8GHz and 2.3GHz respectively. Fig. 3 shows experiment environment with the used radar module. In that environment, we gathered experiment data about a selected number of human, and using the measured data, we compared the performances between the conventional OS-CFAR and proposed detection algorithms. Information about the number of human is not given for evaluating algorithms, and the parameters are same for all the test cases.

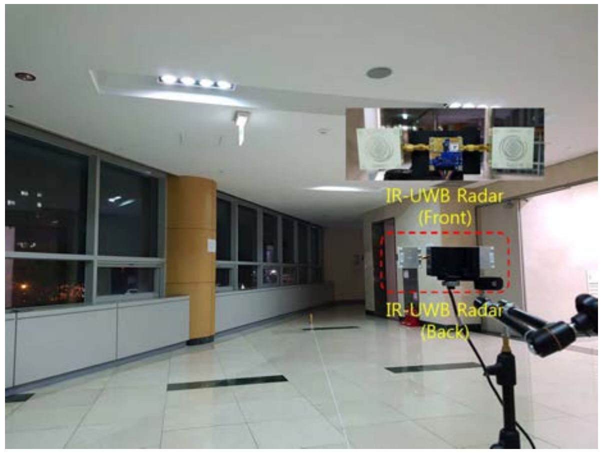

FIGURE 3. Experiment Environment.

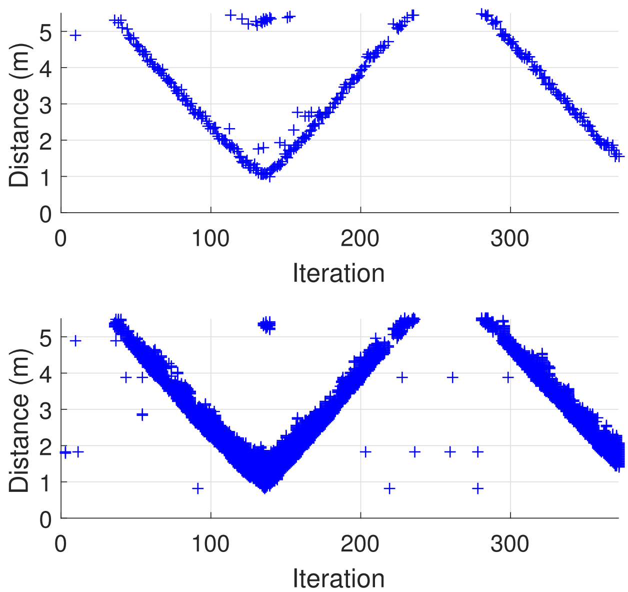

FIGURE 4. Experiment results of the proposed (upper) and conventional CFAR (lower) detection algorithms in case of one moving human target.

Fig. 4 and Fig. 5 show experiment results about a selected number of moving human. x-axis and y-axis represent iteration number and distances of the detected

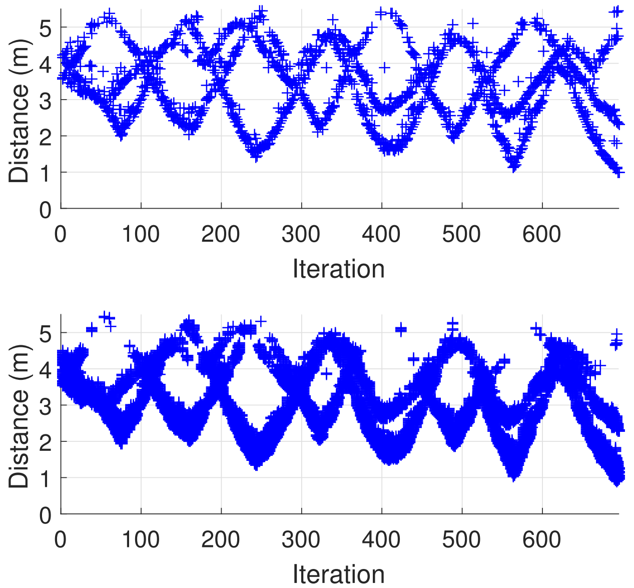

FIGURE 5. Experiment results of the proposed (upper) and conventional CFAR (lower) detection algorithms in case of three moving human targets.

FIGURE 6. Experiment results of the proposed (upper) and conventional CFAR (lower) detection algorithms in case of two near human targets (Distance between human ≈ 70cm).

peaks, respectively. For the first case, a human moved back and forth. The lower sub-figure in the Fig. 4 represents detected peaks by the conventional OS-CFAR detection algorithm. The OS-CFAR algorithm find all the spiky peaks which are reflected by same body, without any clustering scheme. That results in multiple detected traces. When the distance between a human and the radar system decreases, more number of peaks are detected, because the number of different paths from body increases. However, in the upper sub-figure in the Fig. 4, our proposed detection algorithm finds only effective peaks from multiple peaks of a human. Although, we set parameters of t_{left} and t_{right} regarding clustering size as fixed value, the clustering size is spontaneously adjusted according to the size of cluster. It is because that the found peak is regarded as an effective peak only if the peak is local maximum within the clustering size based on proposed detection algorithm. Multiple peaks are clustered by the proposed algorithms, and the noisy peaks by multipath or clutter

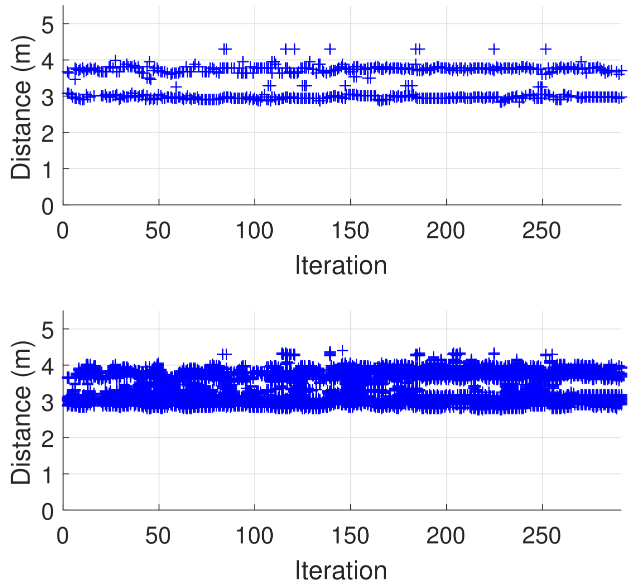

FIGURE 7. Experiment results of the proposed (upper) and conventional CFAR (lower) detection algorithms in case of two near human targets (Distance between human ≈ 50cm).

are rejected by TC method using predetermined threshold value in that environment. The threshold is measured using the environmental parameters in the Table I. In Fig. 5, three human moved. Multiple detected peaks by the conventional OS-CFAR algorithm in the lower sub-figure in the Fig. 5 make a confusion for the recognition of the number of target, and make it difficult to find distance traces of three human. The far human sometimes fail to be detected, because the dense multipath signals of multi-human. It could raise the threshold value of the OS-CFAR algorithm. However, in the upper sub-figure in the Fig. 5, the proper effective peaks of three human are detected. Although we cannot identify the human for each distance, the trace of each human is almost clearly recognized along with the number of human.

To compare distance resolution for the close human, we tested for two and four closely standing human as Fig. 6, Fig. 7, and Fig. 8. In Fig. 6, two human are standing with the distance of about 70cm during this experiment. The traces, which are detected by the OS-CFAR algorithm, of two human are hardly recognized. With our proposed algorithm, the clusters of multi-human are separated, and traces of multi-human are clearly recognized. When there are two human who are standing with the distance of about 50cm as Fig. 7, the OS-CFAR algorithm fail to resolve two close human while our proposed algorithm successively separates two human. Even, in Fig. 8, there are four human and distance between the adjacent human is about 30cm. The four traces of four human are relatively well recognized by the proposed algorithm than the OS-CFAR algorithm. To show more details about the multi-human detection process based on our proposed algorithm behind some selected figures presented here, we have included supplementary multimedia files. These files show

Test environment for 2 near human targets

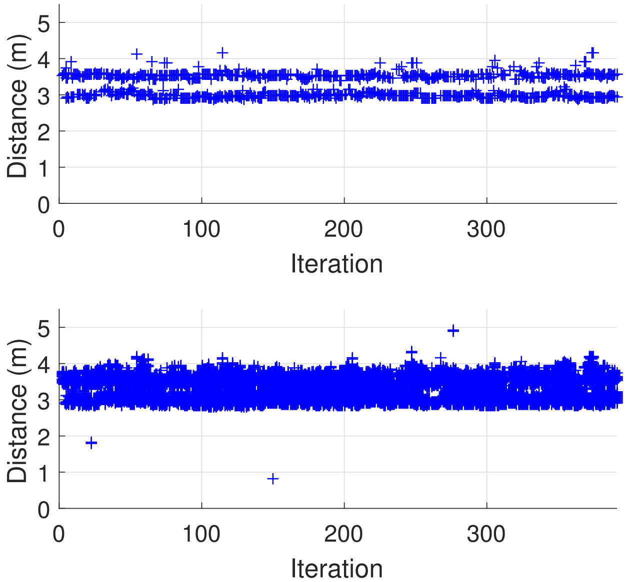

FIGURE 8. Experiment results of the proposed (upper) and conventional CFAR (lower) detection algorithms in case of four near human targets (Distance between human ≈ 30cm).

the process of how to find multiple effective peaks caused by actual people under different scenarios, while comparing the performance with the conventional OS-CFAR detection algorithm. This will be available at http://ieeexplore.ieee.org.

IX. CONCLUSION

We proposed the multi-human detection algorithm based on IR-UWB radar system, especially, by repeatedly performing clustering and detecting processes. With our proposed algorithm, the clusters for multi-human can be separated and the traces of multi-human can be finely recognized. It could be used for indoor positioning system for multi-human based on IR-UWB radar system. In addition, the proposed detection algorithm could be applied to the people counting scenario based on clustering scheme in the preprocessing step for improving performance. Our feature works is to realize people counting and positioning system for multi-human based on the IR-UWB radar sensors.

REFERENCES

[1] M. Navarro and M. Najar, "Toa and DOA estimation for positioning and tracking in ir-uwb," in *Proc. IEEE Int. Conf. Ultra-Wideband*, Sep. 2007, pp. 574–579.

[2] R. Fujiwara, K. Mizugaki, T. Nakagawa, D. Maeda, and M. Miyazaki, "Toa/tdoa hybrid relative positioning system using uwb-ir," in *Proc. IEEE Radio Wireless Symp.*, Jan. 2009, pp. 679–682.

[3] B. Schleicher, I. Nasr, A. Trasser, and H. Schumacher, "IR-UWB radar demonstrator for ultra-fine movement detection and vital-sign monitoring," *IEEE Trans. Microw. Theory Techn.*, vol. 61, no. 5, pp. 2076–2085, May 2013.

[4] F. Khan, J. W. Choi, and S. H. Cho, "Vital sign monitoring of a non-stationary human through IR-UWB radar," in *Proc. 4th IEEE Int. Conf. Netw. Infrastruct. Digit. Content (IC-NIDC)*, Sep. 2014, pp. 511–514.

[5] A. Rabbachin, T. Q. S. Quek, P. C. Pinto, I. Oppermann, and M. Z. Win, "Non-coherent UWB communication in the presence of multiple narrowband interferers," *IEEE Trans. Wireless Commun.*, vol. 9, no. 11, pp. 3365–3379, Nov. 2010.

[6] C. Abou-Rjeily, "Unitary space-time pulse position modulation for differential unipolar MIMO IR-UWB communications," *IEEE Trans. Wireless Commun.*, vol. 14, no. 10, pp. 5602–5615, Oct. 2015.

[7] J. W. Choi, S. H. Cho, Y. S. Kim, N. J. Kim, S. S. Kwon, and J. S. Shim, "A counting sensor for inbound and outbound people using ir-uwb radar sensors," in *Proc. IEEE Sensors Appl. Symp. (SAS)*, Apr. 2016, pp. 1–5.

[8] X. Quan, J. W. Choi, and S. H. Cho, "In-bound/Out-bound detection of people's movements using an IR-UWB radar system," in *Proc. Int. Conf. Electron., Inf. Commun. (ICEIC)*, Jan. 2014, pp. 1–2.

[9] V.-H. Nguyen and J.-Y. Pyun, "Location detection and tracking of moving targets by a 2D IR-UWB radar system," *Sensors*, vol. 15, no. 3, pp. 6740–6762, 2015. [Online]. Available: http://www.mdpi.com/1424-8220/15/3/6740

[10] K. Terasaka, K. Higashikaturagi, I. Matsunami, and A. Kajiwara, "Human body detection using UWB-IR indoor channel," in *Proc. IEEE 18th Int. Symp. Pers., Indoor Mobile Radio Commun.*, Sep. 2007, pp. 1–5.

[11] S. Chang, M. Wolf, and J. W. Burdick, "Human detection and tracking via ultra-wideband (UWB) radar," in *Proc. IEEE Int. Conf. Robot. Autom. (ICRA)*, May 2010, pp. 452–457.

[12] G. Shingu, K. Takizawa, and T. Ikegami, "Human body detection using UWB radar in an indoor environment," in *Proc. Int. Symp. Commun. Inf. Technol. (ISCIT)*, Oct. 2008, pp. 283–288.

[13] A. Kumar, Z. Li, Q. Liang, B. Zhang, and X. Wu, "Experimental study of through-wall human detection using ultra wideband radar sensors," *Measurement*, vol. 47, no. 1, pp. 869–879, 2014. [Online]. Available: http://www.sciencedirect.com/science/article/pii/S0263224113005150

[14] R. Zetik, S. Jovanoska, and R. Thoma, "Simple method for localisation of multiple tag-free targets using UWB sensor network," in *Proc. IEEE Int. Conf. Ultra-Wideband (ICUWB)*, Sep. 2011, pp. 268–272.

[15] H. Wang, G. Wei, T. Wang, and X. Wang, "An improved CFAR for life detection of UWB radar," in *Proc. IEEE 11th Conf. Ind. Electron. Appl. (ICIEA)*, Jun. 2016, pp. 551–554.

[16] A. Maali, A. Mesloub, M. Djeddou, H. Mimoun, G. Baudoin, and A. Ouldali, "Adaptive CA-CFAR threshold for non-coherent IR-UWB energy detector receivers," *IEEE Commun. Lett.*, vol. 13, no. 12, pp. 959–961, Dec. 2009.

[17] A. Maali, A. Mesloub, M. Djeddou, G. Baudoin, H. Mimoun, and A. Ouldali, "CA-CFAR threshold selection for IR-UWB TOA estimation," in *Proc. 7th Int. Workshop Syst., Signal Process. Their Appl. (WOSSPA)*, May 2011, pp. 279–282.

[18] H. Rohling, "Radar CFAR thresholding in clutter and multiple target situations," *IEEE Trans. Aerosp. Electron. Syst.*, vol. AES-19, no. 4, pp. 608–621, Jul. 1983.

[19] D. A. Shnidman, "Radar detection in clutter," *IEEE Trans. Aerosp. Electron. Syst.*, vol. 41, no. 3, pp. 1056–1067, Jul. 2005.

[20] P. P. Gandhi and S. A. Kassam, "Analysis of CFAR processors in homogeneous background," *IEEE Trans. Aerosp. Electron. Syst.*, vol. 24, no. 4, pp. 427–445, Jul. 1988.

[21] V. G. Hansen and J. H. Sawyers, "Detectability loss due to 'greatest of' selection in a cell-averaging CFAR," *IEEE Trans. Aerosp. Electron. Syst.*, vol. AES-16, no. 1, pp. 115–118, Jan. 1980.

[22] R. Viswanathan and A. Eftekhari, "A selection and estimation test for multiple target detection," *IEEE Trans. Aerosp. Electron. Syst.*, vol. 28, no. 2, pp. 509–519, Apr. 1992.

[23] A. F. Molisch, J. R. Foerster, and M. Pendergrass, "Channel models for ultrawideband personal area networks," *IEEE Wireless Commun.*, vol. 10, no. 6, pp. 14–21, Dec. 2003.
[24] L. E. Brennan and F. S. Hill, "A two-step sequential procedure for improving the cumulative probability of detection in radars," *IEEE Trans. Military Electron.*, vol. 9, no. 3, pp. 278–287, Jul. 1965.
[25] H. Zhang, T. Udagawa, T. Arita, and M. Nakagawa, "A statistical model for the small-scale multipath fading characteristics of ultra wideband indoor channel," in *IEEE Conf. Ultra Wideband Syst. Technol. Dig. Papers.*, May 2002, pp. 81–85.
[26] J. Kunisch and J. Pamp, "Measurement results and modeling aspects for the UWB radio channel," in *IEEE Conf. Ultra Wideband Syst. Technol., Dig. Papers.*, May 2002, pp. 19–23.
[27] A. F. Molisch, "Ultra-wide-band propagation channels," *Proc. IEEE*, vol. 97, no. 2, pp. 353–371, Feb. 2009.
[28] D. Cassioli, M. Z. Win, and A. F. Molisch, "The ultra-wide bandwidth indoor channel: From statistical model to simulations," *IEEE J. Sel. Areas Commun.*, vol. 20, no. 6, pp. 1247–1257, Aug. 2002.
[29] R. H. Khan and S. Le-Ngoc, "A singular value decomposition (SVD) based method for suppressing Ocean clutter in high frequency radar," *IEEE Trans. Signal Process.*, vol. 41, no. 3, pp. 1421–1425, Mar. 1993.
[30] M. Piccardi, "Background subtraction techniques: A review," in *Proc. IEEE Int. Conf. Syst., Man Cybern.*, vol. 4. Oct. 2004, pp. 3099–3104.
[31] H. Hindi, "A tutorial on convex optimization," in *Proc. Amer. Control Conf.*, vol. 4. Jun. 2004, pp. 3252–3265
[32] H. S. Wilf, "A global bisection algorithm for computing the zeros of polynomials in the complex plane," *J. ACM*, vol. 25, no. 3, pp. 415–420, Jul. 1978. [Online]. Available: http://doi.acm.org/10.1145/322077.322084
[33] J. M. Kelif, M. Coupechoux, and P. Godlewski, "Effect of shadowing on outage probability in fluid cellular radio networks," in *Proc. 6th Int. Symp. Model. Optim. Mobile, Ad Hoc, Wireless Netw. Workshops (WiOPT)*, Apr. 2008, pp. 141–150.

JEONG WOO CHOI (S'17) received the B.S. and M.S. degrees in electronic engineering from Hanyang University, South Korea, in 2012 and 2014, respectively, where he is currently pursuing the Ph.D. degree. His research interests include signal processing and embedded implementation, especially about, the IR-UWB radar based detection, vital signs, people counting, and positioning.

SUNG SIK NAM (S'05–M'09) received the B.S. and M.S. degrees in electronic engineering from Hanyang University, South Korea, in 1998 and 2000, respectively, the M.S. degree in electrical engineering from the University of Southern California, USA, in 2003, and the Ph.D. degree from Texas A&M University, College Station, TX, USA, in 2009. From 1998 to 1999, he was a Researcher with the Electronics and Telecommunications Research Institute, South Korea. From 2003 to 2004, he was a Manager with the Korea Telecom Corporation, South Korea. From 2009 to 2010 and from 2011 to 2013, he was with Hanyang University and Sungkyunkwan University, South Korea, respectively. Since 2013, he has been with Hanyang University. His research interests include the design and performance analysis of wireless communication system, diversity techniques, power control, multiuser scheduling, cooperative communications, energy harvesting, and free-space optical communication.

SUNG HO CHO (S'86–M'88) received the Ph.D. degree in electrical and computer engineering from The University of Utah, Salt Lake City, UT, USA, in 1989. From 1989 to 1992, he was a Senior Member of Technical Staff with the Electronics and Telecommunications Research Institute, Daejon, South Korea. He was with the Department of Electronic Engineering, Hanyang University, Seoul, South Korea, in 1992, where he is currently a Professor. Since 2008, he has been a recipient of the High-Level Foreign Experts Fellowship from the Beijing University of Posts and Telecommunications, Beijing, China, led by the Ministry of Education of China. His research interests include applied signal processing, machine learning for signal processing, context aware computing, radar sensors, and smart space & wireless network.